MDPI

Article

Paleoenvironmental Implications of Authigenic Magnesian Clay Formation Sequences in the Barra Velha Formation (Santos Basin, Brazil)

Paulo R. A. Netto [1,2,3], Manuel Pozo [3,*], Maurício Dias da Silva [4], Márcia Elisa Boscato Gomes [4], André Mexias [4], Camila Wense Ramnani [5], Yaro Parizek-Silva [5], Leonardo Borghi [2] and Aristóteles de Moraes Rios-Netto [2]

[1] Petrobras S.A., Av. Henrique Valadares, 28, 6th Floor, Rio de Janeiro 20231-030, Brazil; pnetto@petrobras.com.br
[2] Geology Department, Geoscience Institute, Universidade Federal do Rio de Janeiro, Av. Athos da Silveira Ramos 274, Rio de Janeiro 21941-916, Brazil; lborghi@geologia.ufrj.br (L.B.); rios.netto@geologia.ufrj.br (A.d.M.R.-N.)
[3] Department of Geology and Geochemistry, Faculty of Sciences, Universidad Autónoma de Madrid, 28049 Madrid, Spain
[4] Geology Department, Geoscience Institute, Universidade Federal do Rio Grande do Sul, Av. Bento Gonçalves 9500, Porto Alegre 91501-970, Brazil; mauricio95@hotmail.com (M.D.d.S.); marcia.boscato@ufrgs.br (M.E.B.G.); andre.mexias@ufrgs.br (A.M.)
[5] Petrobras Research and Development Center (CENPES), Av. Horácio Macedo 950, Rio de Janeiro 21941-915, Brazil; camila.wense@petrobras.com.br (C.W.R.); yaro@petrobras.com.br (Y.P.-S.)
*   Correspondence: manuel.pozo@uam.es

Abstract: The characterization of Mg-clays in rock samples (well P1) from the Barra Velha Formation (Early Cretaceous) allowed the establishment of mineral assemblages on the basis of their kerolite and Mg-smectite (stevensite and saponite) content. Kerolite-rich assemblages (A and B) rarely contain saponite. Assemblage B is composed of kerolite-stevensite mixed layers, while assemblage A consists of more than 95% kerolite. Mg-smectite-rich assemblages (C and CB) are made up of both Mg-smectites. The predominance of stevensite in the lower interval of the stratigraphic succession suggests evaporative conditions, higher salinity and pH, which would favor its authigenesis by neoformation. In the upper portion, the occurrence of thick kerolite-rich intervals suggests regular water inputs, contributing with a decreasing in salinity and pH, favoring the neoformation of kerolite and later kerolite-stevensite mixed layering. The saponite would be the result of the transformation from Al-smectite into Mg-smectite in a Mg^{2+} rich medium. The results indicate that lake hydrochemical processes would have allowed the establishment of a basic depositional sequence, from base to top, as follows: (i) initial lake expansion stage marked by the occurrence of saponite, (ii) later kerolite neoformation, (iii) formation of kerolite-stevensite mixed layer with increasing salinity, and (iv) neoformation of stevensite, marking a final stage of maximum salinity (evaporation) and alkalinity of the lake.

Keywords: pre-salt; Santos Basin; lacustrine Mg-clays; clay authigenesis; kerolite; stevensite; saponite; diagenesis; mineralogical sequences

1. Introduction

In recent years there has been a resurgence on the topic of magnesian clay minerals, both in their genetic aspects and applications. These minerals give rise to deposits of economic interest in various parts of the world with a wide variety of industrial and technological applications [1–3]. To the above mentioned, we must add the prominence that some of these magnesian clay minerals, mainly kerolite and magnesian smectite, have acquired in the elaboration of models explaining their role in the origin of the huge

oil deposits associated with the pre-salt in an extensive area of the Brazilian coast [2,4]. Although kerolite is not listed as valid specie in the IMA list of minerals, its name is widely used to describe the nanocrystalline, stacking-disordered talc, with a slightly enlarged layer spacing and significant water content [5,6].

For years, many researchers have studied the pre-salt carbonates, especially in the Santos Basin, proposing models about the evolution of the basin and the sedimentary processes that originate these globally unique carbonate formations. The Santos Basin is located southeast of the Brazilian continental margin, between parallels 23º and 28º south, covering 350,000 km^2, up to a bathymetric depth of 3000 m. It includes the coastline of Rio de Janeiro, São Paulo, Paraná and Florianópolis states. It is bounded to the north by the Cabo Frio High and to the south by the Florianópolis High [7]. The formation of the Santos basin took place during the tectonic processes responsible for the breakup of the western supercontinent Gondwana during the Cretaceous, ending with the opening of the South Atlantic Ocean and the separation between South America and Africa [8]. The Santos Basin is classified with other Brazilian and West African basins as passive margin basins [9,10].

In the Santos Basin, the magnesian clays appear very subordinate and associated with a carbonate formation called Barra Velha where stevensite would have formed by neoformation from silica and magnesium-rich gels [11]. This stratigraphic formation was deposited in a lacustrine environment under arid climatic conditions, being composed of a textural variety of carbonates, including laminated, spherulitic and arborescent carbonates, with clays, mostly composed of magnesian clay minerals. Initially, these carbonates were interpreted as deposited under microbial action in a shallow marine environment [12], but subsequently reinterpreted as chemically precipitated in an alkaline lacustrine environment [11,13–17]. The contact between the Barra Velha Formation and the underlying Itapema Formation is an angular unconformity, known as the Pre-Alagoas Unconformity, easily traced in seismic surveys.

Papers concerning the influence of diagenetic and hydrothermal processes on reservoir quality and lithofacies classification, also recognized the presence of magnesian clays, identifying kerolite and magnesian smectite as the most common clay minerals in their study areas [15–17]. Recent studies such as that reported by Mercedes-Martín [18] have proposed a thermodynamic conceptual model to evaluate the role of the hydrological budgets in clay-silica-carbonate alkaline lacustrine precipitation, and its application to the Aptian pre-salt case study.

Wright [11] proposed a basic depositional cycle of carbonates and clays controlled by the hydrochemistry of lake waters. This sequence features from base to top: 1-laminated deposits, 2-magnesian clays and spherulites 3-fascicular calcite. The lithofacies and associated minerals would be related to climatic cycles. In arid conditions, authigenesis of magnesian clay minerals would be favored, followed by precipitation of spherulites and fascicular calcite. In humid conditions there would be input of fresh water favoring silica precipitation and a decrease in the formation of magnesian clays.

However, no sequences of formation of the magnesian clay minerals have been employed to justify their distribution. The main objective of this work is to analyze the variability of magnesian clay minerals recognized in a representative stratigraphic succession from the Aptian Barra Velha Fm to assess the possible paleoenvironmental conditions associated with clay formation in lacustrine environments.

2. Materials and Methods

A total of 75 samples have been collected from well P1 located in the Santos Outer High structure of the Santos Basin (Figure 1). Fifty-seven of those samples were mineralogically characterized by Netto [2], and 18 more samples were collected, and its characterization allowed the establishment of two mineralogical sequences. The samples comprise core, core plugs and side wall cores from Barra Velha Fm. Petrographic thin sections were prepared from 75 samples, impregnated with blue epoxy resin, and stained with Alizarin Red-S solution to aid in the carbonate mineral identification [19].
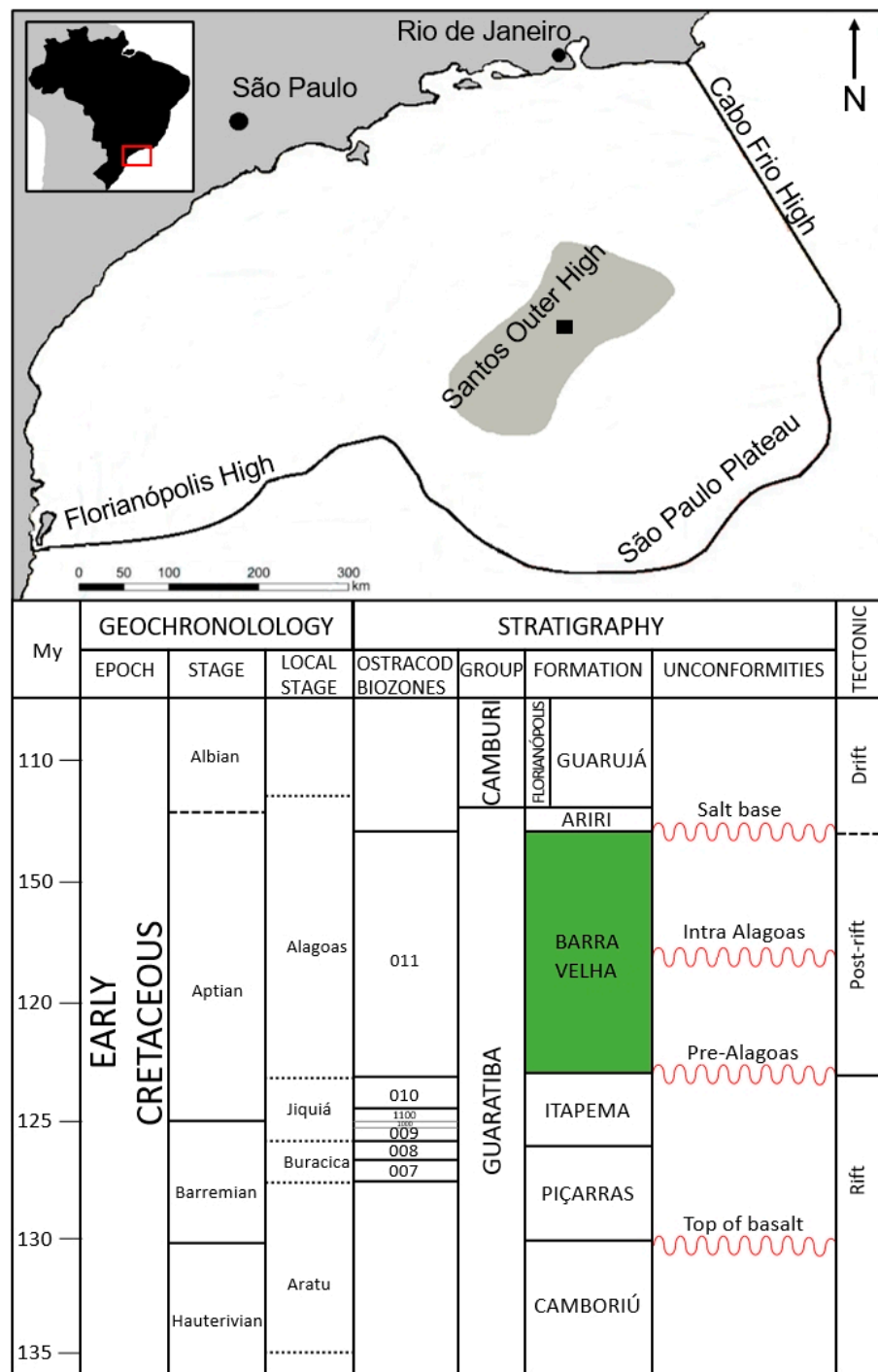
Figure 1. Location of the Santos Basin, offshore Brazil. The black rectangle into the Santos Outer High shows the studying area (modified from [20]). The Lower Cretaceous stratigraphic chart is also shown. The boundaries of Barra Velha Fm are given by Pre-Alagoas Unconformity and Salt Base Unconformity. The Barra Velha Fm is separated into lower and upper by the Intra-Alagoas Unconformity. The Barra Velha Fm was deposited during the Alagoas Local Stage, which is correlated to the Ostracod Biozone 011 [21] (modified from Netto et al. [2]).

Petrographic thin sections from 14 samples were analyzed in a SEM/EDS FEI QUEM-SCAN 605 with acceleration voltage of 15 kV and 5 μm of resolution to generate high-resolution mineral maps which complemented the identification of minerals in thin sections, being especially interesting the phyllosilicates distribution and composition (e.g., Mg-clay minerals vs Al-clay minerals).

Mineralogical analysis of the 75 samples was carried out by means of X-ray diffraction (XRD) in a Rigaku D/MAX–2200/PC equipment (40kV, 34 mA), with a scanning speed of 2.33 °/min for bulk samples (powder method) and 1 °/min for the oriented mounts of clay fraction (<2 μm). The separation of the clay fraction proceeded firstly by the user of a Branson Cell Disruptor—Mod 350 to fragment the samples. Subsequently, several centrifuge steps were performed to separate the clay fraction of the samples (in some cases with low content of clay minerals). After this step, the identification of the clay minerals was carried out on oriented mounts of air-dried sample, with ethylene glycol solvation, and heated at 490 and 550 °C. The mineral intensity factors (MIF) method was applied to XRD reflection intensity ratios normalized to 100% with calibration constants for the semi-quantitative estimation of mineral contents [22–24].

A total of 14 selected samples were examined by scanning electron microscopy (SEM) in a JEOL JSM6490LV equipment, after coating with gold (10 nm thick), operating in high vacuum at 20 kV. Microanalyses were carried out by use of an Oxford energy dispersive spectroscopy (EDS) analyzer attached to the SEM equipment. The microfabric terminology proposed by [25] has been used.

3. Results

3.1. Mineralogical Sequences and Mineral Distribution

Analysis of the hand samples and thin sections allowed the identification of three basic facies proposed by previous works: 1-laminated carbonates, 2-carbonate spherulites and clays, and 3-fascicular carbonate (see [11,15–17]), as well as an intraclastic carbonate facies, formed by reworked fragments of these three previous facies.

The distinction of microfacies was proposed by Netto [2] (Figure 2) and it is equivalent to that described by other authors in the Santos, Campos and Kwanza Basins [4,11,16,17,26,27].
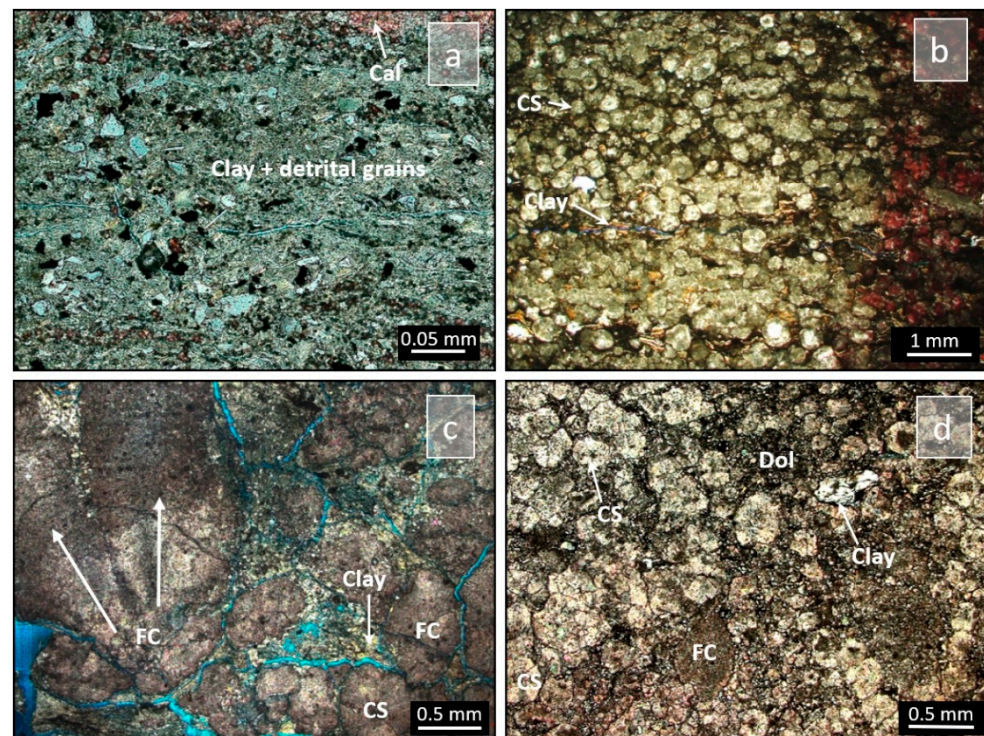
Figure 2. Microfacies. (**a**) Laminated carbonate—MF-1. (**b**) Carbonate spherulites (CS) and clays—MF-2. (**c**) Fascicular (shrub-like) carbonate (FC)—MF-3. (**d**) Intraclastic carbonate—MF-4.

Microfacies MF-1 (Laminate Carbonate) is comprised by alternations of carbonate and clays sheets. Locally, levels of detrital grains are present, imparting an allochthonous character to these levels. MF-2 (Spherulite and Clays) is comprised by laminated clays and calcite spherulites. The spherulite growth take place withing the clay (pseudo matrix) showing two different textures "grain-supported" and "matrix-supported" for coalescent and non-coalescent growth. Microfacies MF-3 (Fascicular—shrub like—Carbonate) is composed of fascicular calcite carbonate with ray crystal shrub fabric (Folk et al., 1985; Chafetz and Guidry 1999), associated to variable content of clays that commonly occurs infilling porosities. Finally, the microfacies MF-4 is comprised by reworked intraclasts of MF-1, MF-2 and/or MF-3 showing both grain-supported and matrix-supported textures. In all microfacies dolomitization and quartz replacement and/or cementation are the main diagenetic features.

The microfacies classification allowed the differentiation of two microfacies types: the in situ and the reworked microfacies (Figure 3). The microfacies interpreted as deposited in situ are carbonate spherulites and clays (MF-2) and fascicular (shrub-like) carbonate (MF-3), which are equivalent to facies F2 and F1, respectively, proposed by Wright and Barnett [11,28]. The laminated carbonates microfacies (MF-1) presents both in situ deposition features and the presence of detrital material, generally siliciclastic (quartz, micas, Al-smectite, rare rock fragments). This microfacies is correlated with facies F3 proposed by Wright and Barnett [28]. The MF-1 microfacies also shows rare features that suggest microbial activity (e.g., nodular calcite, micritized calcite) and are equivalent to the F4 facies suggested by Wright and Barnett [28]. Finally, reworked microfacies come from the remobilization of in situ facies and locally may have siliciclastic components suggesting that the deposition of the reworked microfacies may be the result of sedimentation in the lake shore areas.
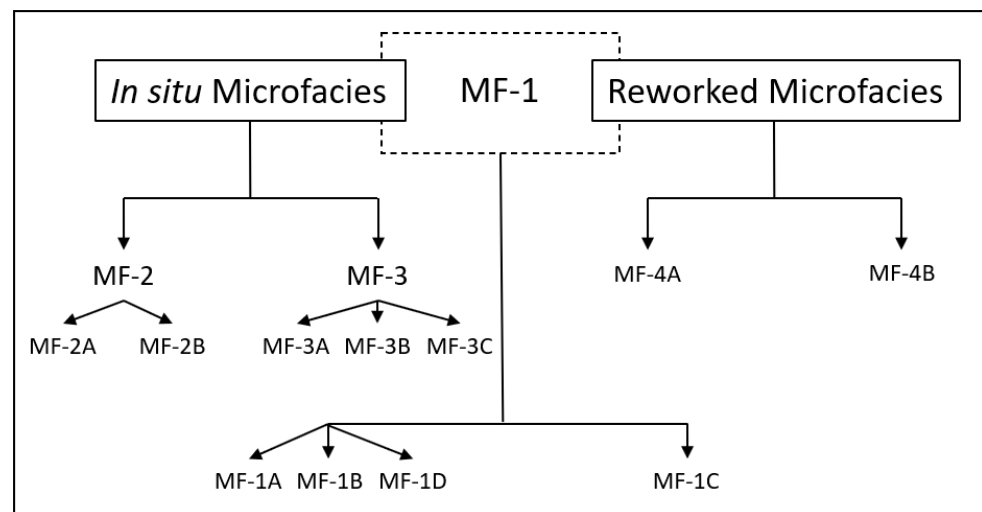
Figure 3. Major microfacies diagram for in situ and reworked facies of the Barra Velha Fm. Microfacies MF-2 and MF-3 are in situ while Mf-4 represents the reworked ones. MF-1 presents both in situ (MF-1A, MF-1B and MF-1D) and mixture of detrital grains, reworked intraclasts and in situ material in the microfacies MF-1C (modified from Wright and Barnett [28]).

These facies follow each other along the interval intersected by the drilling of well P1 (Figure 4e). Detrital grains are recognized in thin sections and are commonly associated to samples showing clay content.
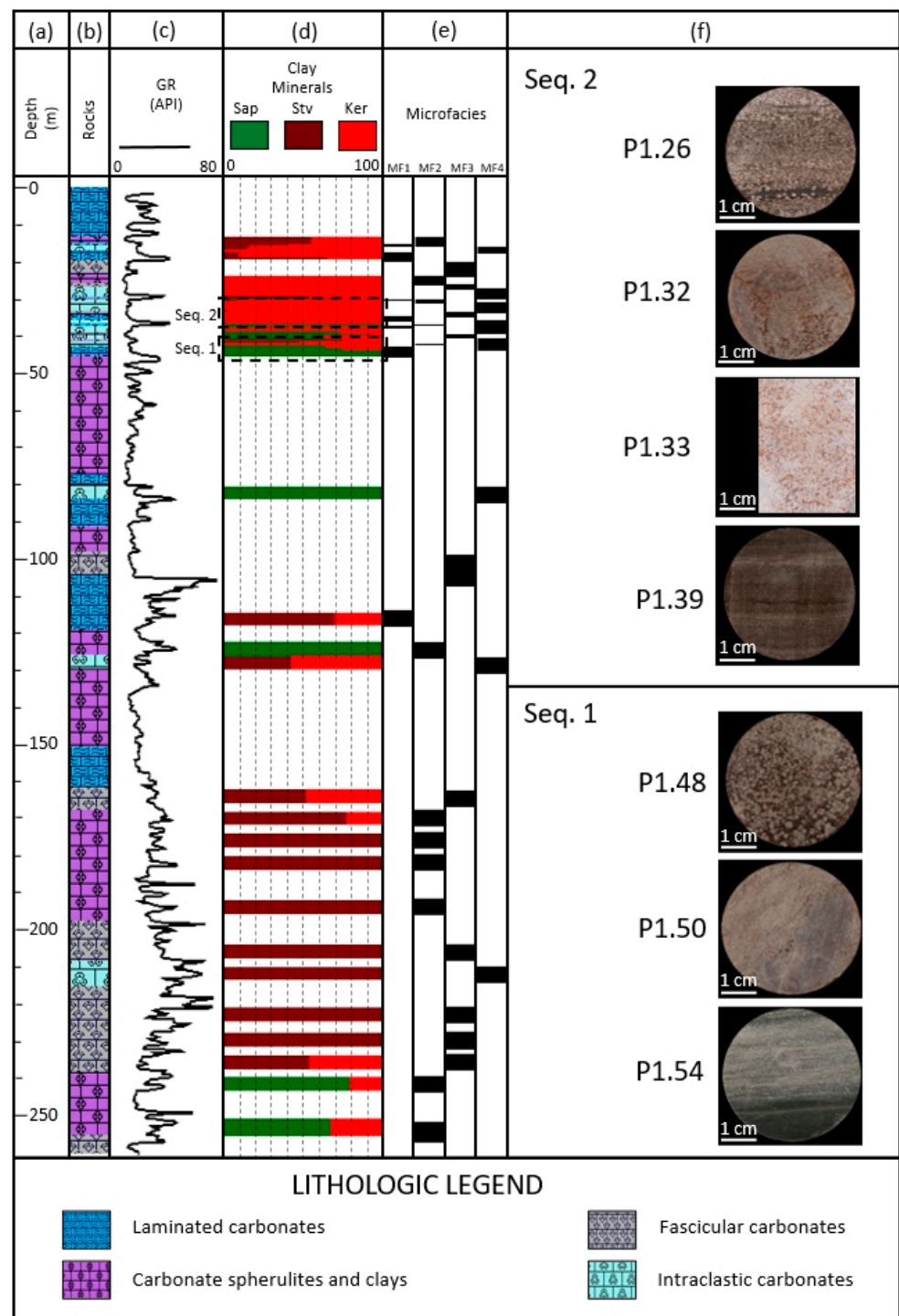
Figure 4. Schematic lithological section from well P1, showing: (**a**) Depth. (**b**) Lithological section. (**c**) Gamma-ray profile. (**d**) Clay mineralogy (the dashed rectangles indicate the mineralogical sequences 1 and 2). (**e**) Microfacies. (**f**) Representative hand samples from the differentiated lithofacies in sequences. Zero-meter depth representing the top of the Barra Velha Fm (modified from [2]).

Figure 4 shows the plot in depth (a) of the lithological Section (b), gamma ray log profile (c), clay fraction with kerolite, saponite and stevensite (d), and microfacies (e).

The gamma ray log shows a slight difference between the well top and bottom. At the top of the interval the gamma ray log shows lower background values alternating with metric to submetric levels with higher values. Intervals composed mainly of kerolite (>95%, assemblage A) presenting thicknesses of up to 10 m occur, generally associated with low

gamma ray values (Figure 4c). These intervals are intercalated with submetric levels which contain more than 95% Mg-smectite (saponite or stevensite) in the clay fraction (assemblage C), and levels with variable contents of Mg-smectite (saponite or stevensite) and kerolite (>50% kerolite—assemblage B, >50% Mg-smectite—assemblage CB), the cited assemblages were proposed by [2] see Table 1. Levels which contain stevensite or saponite [2,4] show correlation with the gamma ray peaks, which may be associated with higher concentration of organic matter (higher U and Th contents) or intervals with detrital grains (e.g., micas, feldspars, and others).

Table 1. XRD determinations of minerals for bulk and clay fraction (<2 μm) samples, interpreted microfacies (MF) and clay assemblages, representatives of the identified mineralogical sequences intervals. Abbreviations: Phy (Phyllosilicate), Qtz (Quartz), Cal (Calcite), Dol (dolomite), Sme (Smectite), Ker (Kerolite), and Ilt (Illite).

Seq.	Samp.	Phy (%)	Qtz (%)	Cal (%)	Dol (%)	Sme (%)	Ker (%)	Ilt (%)	MF	Clay Assemb.
Sequence 2	P1.26	35	2	63	-	90	10	-	MF-2A	CB
	P1.27	25	1	72	2	32	68	Tr	MF-2A	B
	P1.28	22	-	76	1	9	91	-	MF-4A	B
	P1.29	49	4	47	-	-	100	-	MF-4A	A
	P1.30	78	6	15	1	-	100	-	MF-4A	A
	P1.31	48	-	49	3	-	100	-	MF-4A	A
	P1.32	34	-	55	11	7	93	-	MF-4B	B
	P1.33	17	1	77	6	-	100	-	MF-3A	A
	P1.34	19	-	69	12	-	100	Tr	MF-1A	A
	P1.35	27	1	64	8	-	100	-	MF-4B	A
	P1.36	44	-	46	9	-	100	-	MF-4A	A
	P1.37	51	2	43	4	-	100	-	MF-2A	A
	P1.38	21	2	77	1	100	-	-	MF-4B	C
	P1.39	26	2	71	1	100	-	-	MF-1A	C
	P1.40	31	4	64	1	100	-	-	MF-1C	C
Sequence 1	P1.48	34	1	61	5	89	11	-	MF-2A	A
	P1.49	31	1	65	3	48	52	-	MF-4A	B
	P1.50	16	2	76	7	-	100	-	MF-4A	A
	P1.51	16	-	69	15	64	36	-	MF-4A	CB
	P1.52	17	2	55	26	74	26	-	MF-1C	CB
	P1.53	15	12	70	4	100	-	Pr	MF-1C	C
	P1.54	70	7	20	3	100	-	Pr	MF-1C	C

In the lower portion of the well, the correlation between the occurrence of saponite or stevensite and the gamma ray peaks is not that trivial due to the lower sampling rate and the difficulties in depth control of cable sampling tools (side wall cores) compared to the top of the well (cored) and with higher sampling density. However, it is possible to identify a relatively thick interval (approximately 60 m) showing more than 95% stevensite (assemblage C) content in the clay fraction. Unfortunately, the distance between the samples does not allow to stablish a mineralogical sequence analysis as the cored interval does, but clearly it is a thick interval showing stevensite predominance, while the upper portion is richer in kerolite.

The lower interval between samples in the upper section allowed the identification of at least two mineralogical sequences (Figure 4d) which are associated with the chemical variations of the lake water and/or the sedimentological context (open lake or lake margin).

3.2. Mineralogical Sequences

The establishment of mineralogical sequences is fundamental to identifying the lake transgressive and regressive cycles, since these cycles are related to climatic changes influencing the lake hydrochemistry. The hydrochemical features of the lake control the neoformation of magnesian clays (see overview by Pozo and Calvo [1]). Although microorganisms can mediate clay minerals precipitation from solutions (including colloidal components), weathering of silicates, or mediate the transformation of pre-existing phyllosilicates (see overview by Cuadros [29]), no structures were identified to confirm their role in the authigenesis process of the identified magnesian clay minerals. Furthermore, clay minerals of microbial origin tend to have a more variable chemical composition and low crystallinity order than those formed by inorganic processes [30].

3.2.1. Sequence 1 (P1-48 to P1-54)

The first sequence shows the transition from laminated carbonate microfacies (MF-1) to intraclastic carbonate (MF-4), and finally to carbonate spherulite and clay microfacies (MF-2) (Figure 5). It passes from a C assemblage composed of magnesian smectite, interpreted as saponite [2,4], to laminated and intraclastic levels presenting the CB assemblage in which in addition to saponite occurs a low "crystallinity" kerolite (reworked or early neoformed). At the top of the intraclastic level presents assemblage B where kerolite is present with very low ordering ("crystallinity") magnesian smectite interpreted as kerolite-stevensite mixed layers. Stevensite predominates at the top of the sequence showing low kerolite content in the CB assemblage coinciding with the spherulitic microfacies (MF-2).
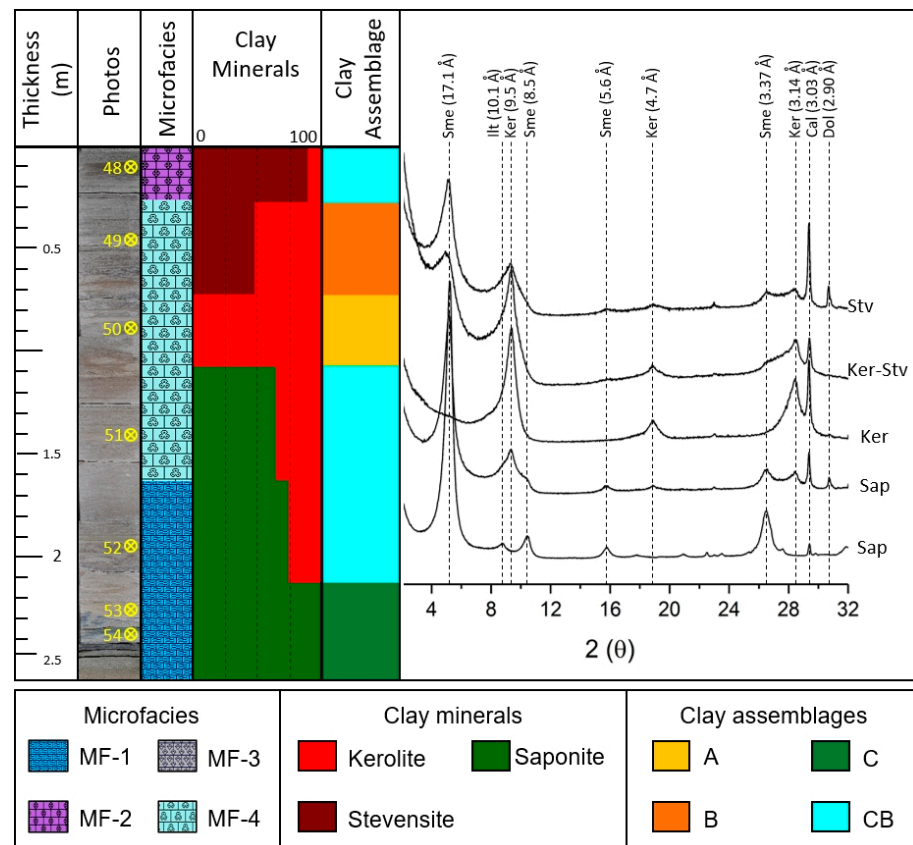
Figure 5. Mineralogical sequence 1. The rocks, clay minerals, assemblages and representative XRD patterns are shown. Ker. Kerolite. Sme (smectite), Ilt (illite), Cal (calcite) and Dol (dolomite).

3.2.2. Sequence 2 (P1-26 a P1-40)

At the base, laminated (MF-1) to intraclastic carbonate microfacies (MF-4) rich in smectite (saponite) are found (assembly C). Upwards spherulitic microfacies (MF-2) kerolite-rich (association A) occurs, with serpentine traces. In the upper kerolitic interval, the laminated (MF-1) microfacies followed by fascicular calcite (MF-3) are shown, passing to the intraclastic microfacies that presents mostly kerolite, with subordinated stevensite (assemblage CB). At the top, the spherulitic microfacies (MF-2) shows evidence of kerolite-stevensite mixed layers, and finally the predominance of stevensite with minor kerolite (assemblage CB) (Figure 6).
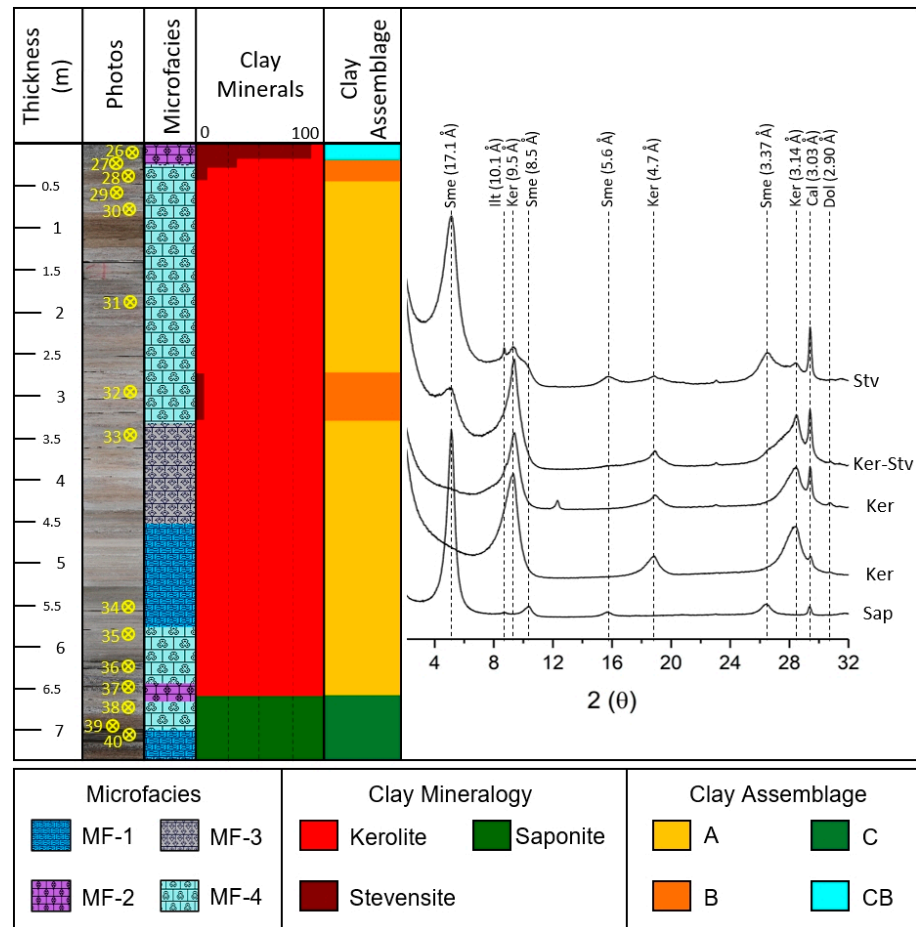
Figure 6. Mineralogical sequence 2. The rocks, clay minerals, assemblages and representative XRD patterns are shown. Ker. Kerolite. Sme (smectite), Ilt (illite), Cal (calcite) and Dol (dolomite).

3.2.3. SEM/EDS High-Resolution Mineral Maps

Mineral mapping by SEM/EDS scanning was performed on thin sections of sequence 2 (Figure 7) by use of QUEMSCAN. In the images it is possible to clearly identify that both dolomitization and silicification occur preferentially replacing Mg-clays. Some bone fragments (apatite) can also be identified.
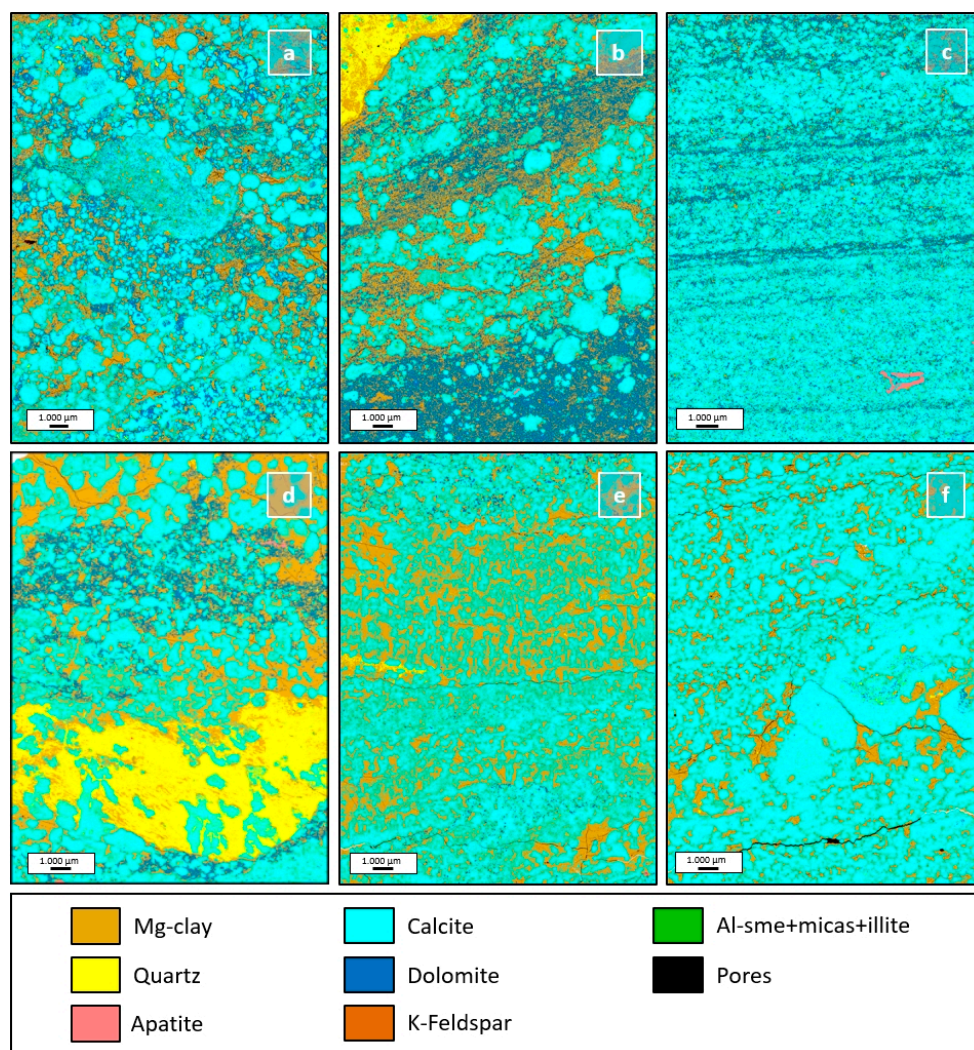
Figure 7. Mineralogical automated mapping analysis in thin sections from the sequence 2. (**a**) sample P1.38, positioned at the bottom of the sequence 2, representative of MF-4 and saponite-rich (assemblage C), showing Mg-clays replacement by dolomite and minor detrital grains. (**b**) sample P1.36 representative of MF-4 kerolite-rich (assemblage A) interval. Shows level of intense quartz replacement and interval where Mg-clays are mainly replaced by dolomite. (**c**) sample P1.34 is representative of a kerolite-rich (assemblage A) Mf-1 microfacies, showing Mg-clays mainly replaced by dolomite. (**d**) sample P1.32 from MF-4 stevensite-rich (assemblage C), showing one zone intensively replaced by quartz and a zone where the Mg-clays present replacement by dolomite. (**e**) sample P1.31 is representative of a kerolite-rich (assemblage A) from MF-4, locally replaced by quartz and dolomite. (**f**) sample P1.27 close to the top of the sequence. It shows kerolite-stevensite mixed layers (assemblage B) with minor replacement of Mg-clays by quartz and dolomite.

Sample P1.38, positioned at the base of sequence 2, is rich in smectite saponite-type (>95%, assemblage C) and is representative of microfacies MF-4 (Figure 7a). Replacement of Mg-clays to dolomite is the main diagenetic process recognized in this sample, although quartz can be identified, it may be mostly related to detrital grains. The sample is mainly composed of calcite (53.2%), Mg-clay (23.6%), dolomite (20.4%) and quartz (2.4%). In addition to these minerals, Al-smectite+micas+illite (<1%) are identified in the sample.

Sample P1.36, also representative of microfacies MF-4 (Figure 7b), is a kerolite-rich sample (>95%, assemblage A). It shows an intensely silicified interval at the top, where both Mg-clays and calcite have been replaced by quartz. Below the silicified zone occur two intervals where the Mg-clays have been replaced by dolomite, especially in the lower

one. The main composition of the sample is calcite (35.7%), Mg-clay (31.6%), dolomite (28.4%) and minor quartz (4.2%).

MF-1 microfacies is represented by sample P1.34 (Figure 7c) in a kerolite-rich interval (assemblage A). In this interval the Mg-clay is strongly dolomitized, and it is possible to identify clay levels almost completely replaced by dolomite. In addition, it is possible to identify areas locally cemented by quartz, and bone fragments. The main composition of the sample is given by calcite (67.4%), dolomite (17.9%), Mg-clay (9.5%) and subordinate quartz (3.9%). Bone fragments are also identified as apatite and it comprises less than 1% of the sample.

Sample P1.32 is another representative sample of MF-4 microfacies (Figure 7d) rich in smectite of stevensite-type (assemblage C). An intensely silicified interval is observed, where both Mg-clay and carbonate are replaced by quartz. This level is positioned between two levels where the dolomitization process affected the Mg-clays. The sample is mainly composed of calcite (40.6%), Mg-clay (29.8%), quartz (19.2%), and dolomite (10.2%).

Sample P1.31 is representative of MF-4 microfacies (Figure 7e) with kerolite predominance (assemblage A). It locally shows Mg-clay replaced by quartz and a level where replacement by dolomite occurs. The sample is composed mainly of calcite (55.3%), Mg-clay (36.1%), with subordinate dolomite (4.2%) and quartz (4.1%).

Sample P1.27 is representative of MF-2 microfacies (Figure 7f) in an interval that shows mixed layers of kerolite-stevensite (assemblage B). It is possible to identify silicification and dolomitization occurring locally. The sample is composed mostly of calcite (76.2%), Mg-clay (19.8%), quartz (2%) and dolomite (1.4%).

3.2.4. Microfabric and SEM-EDS Analyses

SEM-EDS analyses were performed on rock fragments representative of the mineralogical assemblages [2] (Figure 8). The mineralogical assemblages show matrix-type clay-rich microfabric, in addition to deformation features typical of compaction.
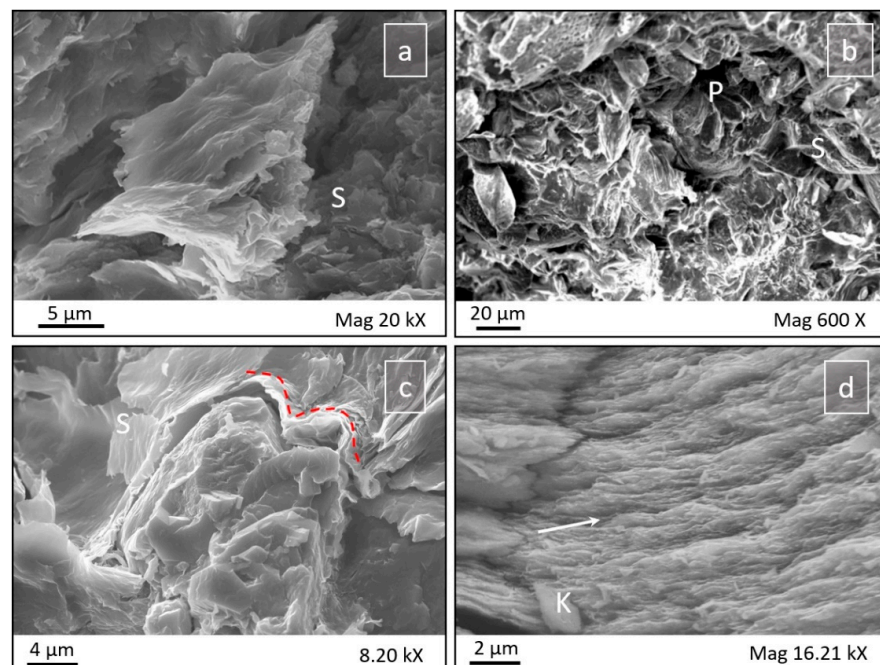
Figure 8. SEM images representative of the sequence intervals. (**a**) Assemblage B representative sample showing matrix-type microfabric and laminar aggregates with wrinkled edges (S). (**b**) assemblage C saponite-rich representative sample, showing matrix-type microfabric, wrinkled edges of smectite (S) and incipient porosity (P). (**c**) shows lamellar smectite (S) in a matrix-type microfabric. The red dashed line shows a deformed microlaminated feature. (**d**) shows a detail of the laminated clay insert of kerolite-rich (assemblage A) showing face-to-face arrangement and deformation by compaction.

Sample P1.49 is representative of the microfacies MF-4 with kerolite-stevensite mixed layers (assemblage B), showing a matrix-type clay-rich microfabric and aggregates of deformed wrinkled lamellae, with smectite appearance (Figure 8a). The Al_2O_3 content, from point EDS analysis varies between 1 and 3% in this assemblage (Table 2).

Table 2. Average ranges of chemical EDS point analyses (oxide wt%) from representative samples of the different assemblages established. Kerolite (Ker), stevensite (Stv) and saponite (Sap).

Analysis	Assemblages					
	A	**B**	**C**		**CB**	
	Ker	**Stv**	**Stv**	**Sap**	**Stv**	**Sap**
SiO_2	60–61	59–62	62–63	57–66	61–66	59–62
Al_2O_3	0–1.08	1–3	0	3–5	0–1.02	3–6.5
MgO	31–32	29–31	23–32	29–33	28–32	27–32
CaO	0–0.83	0–1	0	0.54–2	0	0.4–2
Na_2O	3–3.08	2–3	0.7–2	1.64–3	0.6–2	3–4
K_2O	0	0–0.7	0	1.85	0–2	0
FeO	0	0–0.5	0	0–1.24	0	0

Sample P1.40 is a saponite-rich (assemblage C) (Figure 8b), representative of the microfacies MF-1 (Figure 8b), in addition to the matrix-type microfabric, shows laminar and skeletal microfacies, the latter featuring detrital minerals such as muscovite and biotite, among others, which shows high contents of Al_2O_3 (18-22%) and K_2O (14-18%). The point EDS analysis of the Mg-smectites shows Al_2O_3 contents varying between 3 and 5%.

The sample P1.38 is representative of the microfacies MF-4 with smectite predominance (assemblage C). It shows a detail of deformed laminae (red dashed line) of smectite from saponite-type (S) with laminar morphologies coating carbonate (Figure 8c).

Sample P1.35 of exclusively kerolite (k) composition (assemblage A), generally presents a face-to-face arrangement (Figure 8d), with frequent deformation of the clay by compaction. Locally, the honeycomb microfabric can be observed [2]. Point EDS analyses of the Mg-clay in kerolitic samples, like P1.35, show low Al_2O_3 values reaching a maximum of 1.08% (Table 2).

4. Discussion

Wright [27] discusses the sedimentological model from the identification of basic cyclothems occurring in the Barra Velha Fm [11], proposing that they would represent cycles of flooding and evaporation. In the first moment there would be inflow of fresh water, probably run-off water, which would decrease the salinity-alkalinity and would deepen the lake (expansion). In these lower salinity-alkalinity conditions, the lake could become colonized by ostracods and vertebrates, mainly nearby streams, while below the wave base, carbonate mud may be deposited (laminated carbonates), in addition to silica deposition (triggered by the reduced alkalinity). With water residence time, salinity-alkalinity gradually increase, interstitial silica gels can develop, followed by deposition of Mg-silicate gels overlying the laminated carbonates [14,31] in high-alkalinity waters (pH > 10). The spherulites would grow within the Mg-silicate gel and could be the seed of fascicular (shrub-like) calcite, supported by hybrid forms between spherulites and shrubs identification [15,16,32]. Some shrubs with good porosity show evidence that they probably had Mg-clays matrices. It is possible that this matrix would have been removed by wave action as a result of progressive shallowing [27]. Otherwise, shrubs would be nucleated above the wave base surface in a higher energy, shallower facies environment [14]. The carbonate and clay factory of the Barra Velha Fm can also be influenced by microbial mediation. Microbial mats would favor deposition of laminated carbonates alternating with wavy Mg-clay sheets [33,34]. Nevertheless, microbialites, in the sense of Burne and Moore [35], were not recognized in the petrographic study. The growth of spherulites, shrubs, and coalesced forms can be influenced by microorganisms [34,36,37]. Laboratory

experiments show the growth of radial-spherular calcite in saline and alkaline solutions in the presence of organic acids [38]. Spherulites and coalesced forms were observed when alginic acid even in low salinity solution [39]. The formation of kerolite along with varying amounts of smectite, and the formation of sepiolite and palygorskite, may be associated with extracellular polymeric substances (EPS) in modern environments [40–42]. Stevensite formation is reported to be associated with thrombolites in low saline water of the Lake Clifton [43]. Although evidence of microbial mediation as the main depositional mechanism that has been reported locally in the Barra Velha Fm, the data set analyzed shows no indication of biological mediation for the formation of carbonates or Mg-clay. No evidence of microbial texture or nucleation by bacteria was found in the spherulites. Trapping and binding or branching structures, among others that would indicate microbial mediation [35,44], were not found in the shrubs. Microorganism activity in the formation of Mg-clay also does not seem to have occurred due to their high ordering crystallinity and the absence of microbial structures.

Regarding the carbonate factory and the deposition of magnesian silicates, Netto et al. [2] proposed that laminated carbonates (MF-1) would have been deposited intercalated with Mg-clay and/or inherited minerals in relatively deeper waters, while Mg-rich spherulites (MF-2) (dolomite and/or Mg-calcite) associated with Mg-clays would have formed from the replacement of Mg-clays during eodiagenesis. The shrubs (MF-3) would have grown within the Mg-clays as a product of abiotic chemical precipitation like ray-crystal shrubs in hot-spring travertine depositional systems [45–47]. The described facies are consistent with deposition in a lacustrine environment and would agree with the sedimentological and geochemical cycles identified by Wright and Barnett [11]. Nevertheless, both models are limited in identifying climatic cycles, since identified facies can occur under wet or arid climate if hydrochemical conditions do not change drastically. Even the presence of quartz and chalcedony that could indicate freshwater input [28] can be explained by the amount of non-stoichiometric silica in the initial structure of Mg-silicate gels that can be released as the material becomes more crystalline [48,49].

The identification of mineralogical sequences can contribute significantly to the more precise identification of these flooding and evaporation cycles, since two main processes are involved in the authigenesis of clay minerals [1,50–53]: (i) formation by direct precipitation from solution (neoformation), and (ii) development by transformation of precursor phases, e.g., pyroclastic materials and detrital clays.

The identification of saponite [2,4] in samples associated with the presence of illite, presenting reflection 001 at near 10 Å (Figures 5 and 6), and the occurrence of detrital grains, indicates a different geochemical pathway formation than that suggested for the formation of kerolite and stevensite.

Direct precipitation from a solution containing simple or complex ions involves crystallization of a new mineral, so no preexisting mineral structure is "inherited". Mineral formation from solution is controlled mainly by kinetics. The model of the kinetics of nucleation and growth of minerals was established by Galán and Pozo [54]. Two processes explain the precipitation of a mineral from water: nucleation and subsequent crystal growth. Nucleation is properly produced when a solution is supersaturated with respect to a particular solid or mineral phase [55]. This type of nucleation from aqueous solution is called homogeneous, in contrast to that which occurs on the surface of a preexistent solid (heterogeneous nucleation). Once nucleation has taken place, crystal growth can take place by adding ions and/or molecules to the surface of the crystal nuclei ("classical" crystal growth) [54] or by aggregating and subsequently bonding the crystal nuclei to each other ("nanoparticle" behavior) [53,56].

In this context, both kerolite and stevensite should be a result of authigenesis by neoformation [57–59]. The strong homogenization of the textures of the Mg-clays, possibly due to the degree of diagenesis in the Santos basin, makes it difficult to differentiate them. Nevertheless, it is possible that the nucleation kinetics of kerolite and stevensite were homogeneous.

The formation of authigenic clay minerals by transformation of precursor phases has been termed "neoformation by addition" [50]. The mechanisms involved remain a matter of debate, with several hypotheses being proposed [60]. More recently, an update of the subject has been provided by Tosca [53], pointing out the diffuse boundaries between the mechanisms of epitaxy (precipitation on preexisting natural surfaces) and topotaxy (transformation and reaction of pre-existing surfaces) as processes leading to formation of authigenic Mg-silicates after detrital clay precursors. A detailed review on authigenesis in minerals was reported by Pozo and Calvo [1]. The saponite, in turn, is interpreted as being neoformed by topotaxic transformation of detrital Al-smectites in a Mg^{2+} rich medium or weathering of mafic rocks, which would come from stream water events or moments of higher humidity between long periods of aridity. However, direct neoformation from solution cannot be ruled out, depending on the available Al-particle content.

The mineralogical assemblages identified do not show a specific correlation with the interpreted microfacies, i.e., kerolite- or smectite-rich assemblages can occur in any of the microfacies. This suggests that the deposition/neoformation of Mg-clays is more correlated to the hydrochemistry of the lake than the cyclothems identified by Wright and Barnett [11] in their various papers on pre-salt sedimentation, whose model, while considering the cycles of flooding and evaporation, also correlates the facies to the bathymetry/energy of the system, e.g., shrubs are nucleated above the base of wave action or would be placed in this energy range during periods of greater lake shrinkage (evaporative period). The spherulitic facies would be formed in an intermediate period, between maximum lake shrinkage and maximum expansion, while the laminated carbonates would be representative of the periods of maximum expansion (maximum flooding, deeper water lake). The lake water chemistry would be the key to whether or not Mg-silicate gels occur.

On the other hand, the identification of mineralogical sequences (Figures 5 and 6) shows a greater dependence on the hydrochemical conditions of the lake, since the formation of magnesian clays is mainly controlled by alkalinity (pH), salinity and $p(CO_2)$ [61]. The stability relationships of hydrated Mg-silicates in relation to solute activities indicates that the equilibria between sepiolite, stevensite and kerolite depend on salinity (Na^+ concentration), pH and Mg^{2+} concentration [18,51]. High salinity favors the formation of stevensite while sepiolite and kerolite form under lower salinity conditions, where sepiolite formation is favored when the Si^{4+}/Mg^{2+} ratio is higher. An increase in pH and Mg content in the solution is more favorable for kerolite precipitation, which can explain the lack of sepiolite in the analyzed samples. The metastability of kerolite relative to sepiolite was corroborated experimentally by Stoessell [62].

Sequences 1 and 2 (Figures 5 and 6) show that there is a basic sequence for sedimentation of the Mg-clays that starts with cyclic inputs of detrital material, in particular Al-smectites and illite-mica (flooding period) followed by kerolite and stevensite neoformation (evaporative period).

Sequence 1 shows in the base, an input of inherited saponite and/or Al-smectite, which in a Mg^{2+} rich environment is transformed into saponite, is usually associated with detrital grains. There may be evidence of illite at near 10 Å in assemblage C, overlain by gradual intercalation between saponite and kerolite in assemblage CB, implying kerolite neoformation or reworking, which should be predominant in the spherulitic microfacies (assemblage A), which is overlain by the kerolite-stevensite mixed layers (assemblage B), both indicating increasing salinity and pH. Finally, with even higher salinity, in addition to a high Mg^{2+}/Si^{4+} ratio, the predominance of stevensite occurs, indicating that the lake is in a period of maximum evaporation. The same pattern occurs in sequence 2.

This model is in agreement with the experimental work of Tosca and Masterson [63] which indicate that at a temperature of 25 °C and low salinity (NaCl = 0.0 mol/kg), at pH > 8.7 and a high Mg^{2+}/Si^{4+} ratio the formation of kerolite is favored, although in lower proportions if pH is higher than 9.0. Whereas at a relatively high salinity (NaCl = 0.46 mol/kg) and high Mg^{2+}/Si^{4+} ratio the formation of kerolite and stevensite are favored as a function of pH, where higher pHs favor stevensite.

It is noteworthy that this interval is marked by the presence of quartz and chalcedony, which may mark the greater influx of water with higher SiO_2 concentration in the lake or this excess is a result of the release of non-stoichiometric Si from the initial Mg-silicate gels structure with increasing crystallinity [48,49], given that the kerolite found in the Santos Basin pre-salt shows a higher ordering ("crystallinity") than that found in the Madrid Basin [2].

Several authors have tried to present a model for the deposition of the Barra Velha Formation and, in general, there is the understanding that the lakes would be hyper-alkaline and with high salinity. The causes, however, are still controversial. Some hypotheses have been invoked to explain a persistent high pH in a lake system: (i) input of mantle CO_2 into the lake waters [27,28,64], or (ii) reduced infiltration rates of lake waters into ground water aquifers [18]. In addition, it is suggested that the sources of Ca^{2+}, Mg^{2+} and SiO_2, among others would come from the leaching and chemical weathering of basalts by phreatic and hydrothermal waters [65], and felsic rocks in a very extensive, shallow and endorheic lake [21]. The observation of a basic sequence of deposition of magnesian clays controlled by the hydrochemistry of the lake shows that the contribution of several sources is responsible for the deposition of the Barra Velha Formation.

A simplified general geological and hydrological model for the deposition of the Barra Velha Formation can be seen in Figure 9a (modified from Pietzsch [21]), it is suggested that the sources of ions to the lake may come from drainage (runoff and stream water), ground water, and convection circulation throughout deep fault zones.

According to this model, the base of the cycles was set at the periods of lake expansion and wet periods, when water plus sediments from various source areas are discharged into the lake. At this time, the contribution of silica-laden groundwater recharge can be even more relevant. The deposition of detrital grains rich in Al-smectites, later transformed to saponite [2,4], may occur in distal areas, being deposited interbedded with laminated carbonates and/or together with reworked material from marginal lake sites. In addition, the relative dilution of lake water, reducing its alkalinity and salinity, would favor kerolite deposition in the early stage of lake evolution (Figure 9b). With the establishment of more arid climate and decreasing freshwater inputs to the lake, the evaporative stage begins, where salinity and pH tend to increase, which would favor the neoformation of stevensite [66,67], which could also be favored by Mg^{2+} depletion [68], resulting in the formation of random mixed layers (Figure 9c). Finally, in the maximum shrinkage stage dry weather sets in, increasing the salinity of the lake and favoring the neoformation of stevensite (Figure 9d).
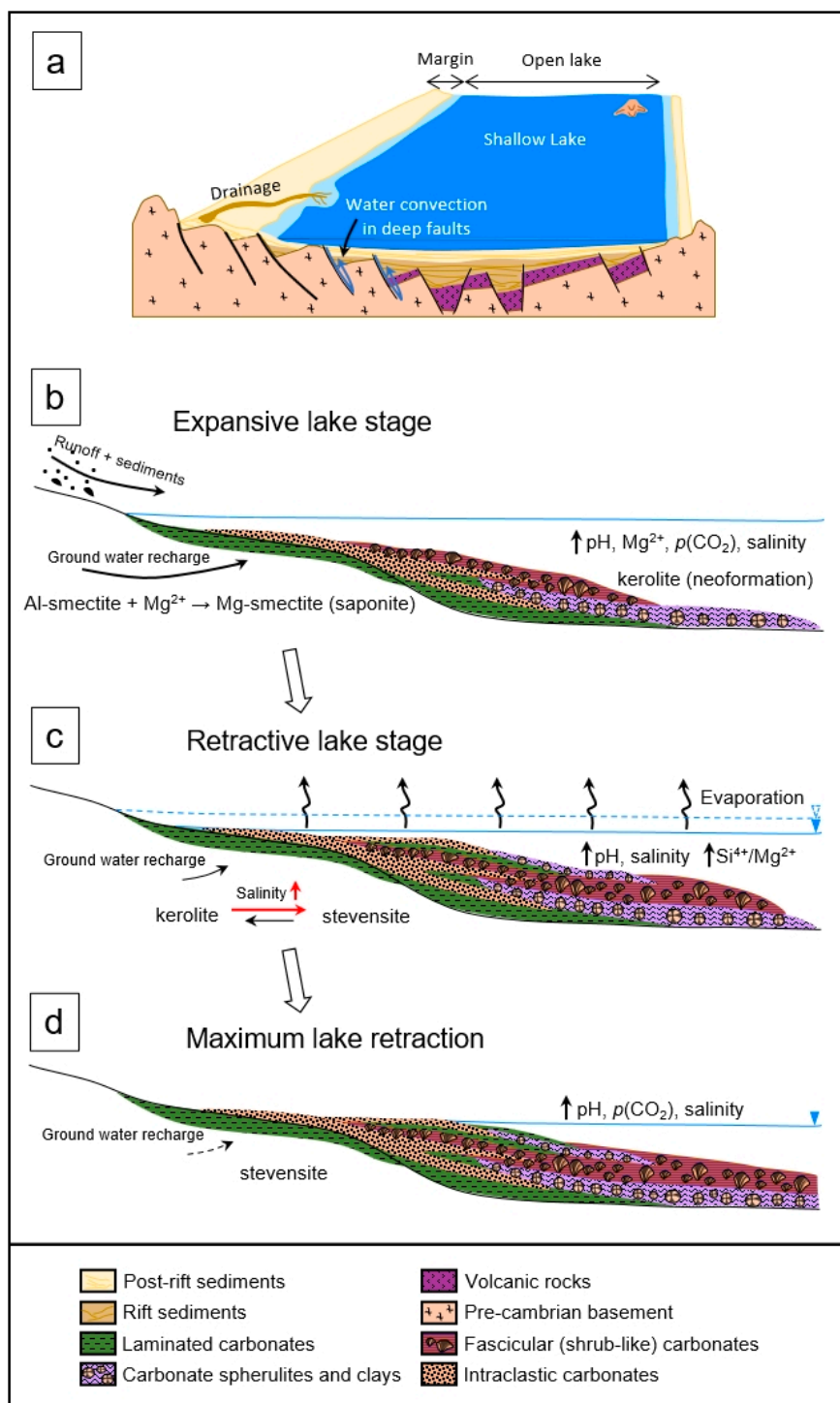
Figure 9. Scheme showing the conceptual depositional model for the post-rift stage, including main Mg-clay minerals authigenic pathways. (**a**) shows a simplified conceptual model illustrating the geology and hydrology of the Barra Velha Fm as a large and shallow endorheic lake (modified from Pietzsch [21]). (**b**) illustrate the expansive lake stage with runoff water and sediment discharge plus ground water contributing to lake water dilution favoring the neoformation of saponite by transformation of Al-smectite in a high Mg^{2+} environment. (**c**) shows the retractive lake stage with a relative low salinity favoring the neoformation of kerolite. Variations in the salinity can favor neoformation of stevensite or generate kerolite-stevensite mixed layers. (**d**) represents the maximum lake retraction with high pH and salinity favoring stevensite neoformation (Modified from Netto [2]).

5. Conclusions

The vertical distribution of established mineralogical assemblages is not homogeneous, with Mg-smectite-rich assemblages being observed in the lower portion, while kerolite-rich ones are found in the upper portion which may be associated with 1st to 3rd order stratigraphic cycles. The recognition of Mg-clay deposition sequences controlled by the lake hydrochemical features, allows the suggestion of a sedimentological model for the studied area. The base of the cycle would be fixed at the lake expansion stage (flood period), being characterized by the occurrence of saponite, which may be associated with laminated carbonates in deeper regions or intraclastic carbonates in shallower environments, while in shallow open lake environments kerolite neoformation could take place locally. The representative assemblages of this stage are C and CB, with local assemblage A. The lake expansion stage would be followed by the initial lake shrinkage stage with onset of the arid period, represented by kerolitic assemblages (A and B), initially characterized by exclusive deposition of kerolite, but also by neoformation of stevensite in mixed layers with kerolite. Finally, the stage of maximum shrinkage with the predominance of stevensite neoformation, with the representative assemblages of C and CB.

Saponite formation would result from the transformation of detrital Al-smectites in a Mg-rich medium. Kerolite and stevensite would be neoformed under the control of the lake's hydrochemical variations, where kerolite would be formed at times of lake water dilution (lower salinity and pH), while higher salinity and/or decreased Mg^{2+} concentration would lead to the formation of mixed kerolite-smectite layers. The levels with stevensite predominance would be formed at times of very high salinity (maximum lake retraction).

The occurrence of silicification was observed mainly in the samples from the upper portion of the well and was generally associated with kerolitic assemblages. This may indicate that the presence of silica is associated with silica-laden groundwater recharge and can be correlated with eodiagenesis in humid periods, as can the occurrence of saponite and the kerolite-stevensite mixed layers. The homogenization of the Mg-clays textures into laminar, may have occurred during compaction. This process may also have been aided by the dolomitization observed in most of the analyzed samples. Further studies would be conducted to understand the effects of burial diagenesis.

Author Contributions: Conceptualization, P.R.A.N. and M.P.; Formal analysis, P.R.A.N.; Investigation, P.R.A.N. and M.P.; Methodology, P.R.A.N. and M.P.; Resources; P.R.A.N., M.D.d.S., C.W.R. and Y.P.-S.; Supervision, M.P., A.M., M.E.B.G., L.B. and A.d.M.R.-N.; Writing—original draft, P.R.A.N.; Writing—review & editing, M.P. All authors have read and agreed to the published version of the manuscript.

Conflicts of Interest: The authors declare no conflict of interest.

References

1. Pozo, M.; Calvo, J. An Overview of Authigenic Magnesian Clays. *Minerals* **2018**, *8*, 520. [CrossRef]
2. Netto, P.R.A.; Pozo, M.; da Silva, M.D.; Mexias, A.S.; Gomes, M.E.B.; Borghi, L.; Rios-Netto, A.M. Authigenic Mg-Clay Assemblages in the Barra Velha Formation (Upper Cretaceous) from Santos Basin (Brazil): The Role of Syngenetic and Diagenetic Process. *Appl. Clay Sci.* **2021**, *216*, 106339. [CrossRef]
3. Cuevas, J.; Ruiz, A.; Fernández, R.; González-Santamaría, D.; Angulo, M.; Ortega, A.; Torres, E.; Turrero, M. Authigenic Clay Minerals from Interface Reactions of Concrete-Clay Engineered Barriers: A New Perspective on Mg-Clays Formation in Alkaline Environments. *Minerals* **2018**, *8*, 362. [CrossRef]
4. da Silva, M.D.; Gomes, M.E.B.; Mexias, A.S.; Pozo, M.; Drago, S.M.; Célia, R.S.; Silva, L.A.C.; Netto, P.; Gomes, L.B.; Porcher, C.C.; et al. Mineralogical Study of Levels with Magnesian Clay Minerals in the Santos Basin, Aptian Pre-Salt Brazil. *Minerals* **2021**, *11*, 970. [CrossRef]
5. Pozo, M.; Galán, E. (Eds.) Magnesian Clay Deposits: Mineralogy and Origin. In *Magnesian Clays: Characterization, Origin and Applications*; AIPEA Educational Series; Digilabs: Bari, Italy, 2015; ISBN 978-88-7522-093-8.
6. Brindley, G.W.; Bistt, D.L.; Wan, H.-M. The Nature of Kerolite, Its Relation to Talc and Stevensite. *Mineral. Mag.* **1977**, *4*, 443–452. [CrossRef]
7. Moreira, J.L.P.; Madeira, C.V.; Gil, J.A.; Machado, M.A.P. Bacia de Santos. *Bol. De Geociências Da Petrobras* **2007**, *15*, 531–549.
8. Pereira, M.J.; Macedo, J.M. A Bacia de Santos: Perspectivas de Uma Nova Província Petrolífera Na Plataforma Continental Sudeste Brasileira. *Bol. De Geocienc. Da Petrobras* **1990**, *4*, 3–11.
9. Carminatti, M.; Dias, J.; Wolff, B. From Turbidites to Carbonates: Breaking Paradigms in Deep Waters. In Proceedings of the All Days, Houston, TX, USA, 4 May 2009; OTC: Houston, TX, USA, 2009.
10. Milani, E.J.; Rangel, H.D.; Bueno, G.V.; Stica, J.M.; Winter, W.R.; Caixeta, J.M.; Pessoa-Neto, O.C. Bacias Sedimentares Brasileiras: Cartas Estratigráficas—Introdução. *Bol. De Geociências Da Petrobras* **2017**, *15*, 183–205.
11. Wright, V.P.; Barnett, A.J. An Abiotic Model for the Development of Textures in Some South Atlantic Early Cretaceous Lacustrine Carbonates. *Geol. Soc. Lond. Spec. Publ.* **2015**, *418*, 209–219. [CrossRef]
12. Terra, G.J.S.; Spadini, A.R.; França, A.B.; Sombra, C.L.; Zambonato, E.E.; Juschaks, L.C.S.; Arienti, L.M.; Erthal, M.M.; Blauth, M.; Franco, M.P.; et al. Classificação de Rochas Carbonáticas Aplicável Às Bacias Sedimentares Brasileiras. *Bol. De Geociências Da Petrobras* **2010**, *18*, 9–29.
13. Tosca, N.J.; Wright, V.P. The Formation and Diagenesis of Mg-Clay Minerals in Lacustrine Carbonate Reservoirs. In Proceedings of the Adapted from oral presentation given at 2014 AAPG Annual Convention and Exhibition, Houston, TX, USA, 6–9 April 2014.
14. Wright, P.; Tosca, N. A Geochemical Model for the Formation of the Pre-Salt Reservoirs, Santos Basin, Brazil: Implications for Understanding Reservoir Distribution. *AAPG Annu. Conv. Exhib.* **2016**, *51304*, 1–32.
15. Herlinger, R.; Zambonato, E.E.; de Ros, L.F. Influence of Diagenesis on the Quality of Lower Cretaceous Pre-Salt Lacustrine Carbonate Reservoirs from Northern Campos Basin, Offshore Brazil. *J. Sediment. Res.* **2017**, *87*, 1285–1313. [CrossRef]
16. Lima, B.E.M.; de Ros, L.F. Deposition, Diagenetic and Hydrothermal Processes in the Aptian Pre-Salt Lacustrine Carbonate Reservoirs of the Northern Campos Basin, Offshore Brazil. *Sediment. Geol.* **2019**, *383*, 55–81. [CrossRef]
17. Gomes, J.P.; Bunevich, R.B.; Tedeschi, L.R.; Tucker, M.E.; Whitaker, F.F. Facies Classification and Patterns of Lacustrine Carbonate Deposition of the Barra Velha Formation, Santos Basin, Brazilian Pre-Salt. *Mar. Pet. Geol.* **2020**, *113*, 104176. [CrossRef]
18. Mercedes-Martín, R.; Ayora, C.; Tritlla, J.; Sánchez-Román, M. The Hydrochemical Evolution of Alkaline Volcanic Lakes: A Model to Understand the South Atlantic Pre-Salt Mineral Assemblages. *Earth-Sci. Rev.* **2019**, *198*, 102938. [CrossRef]
19. Dickson, J.A.D. A Modified Staining Technique for Carbonates in Thin Section. *Nature* **1965**, *205*, 587. [CrossRef]
20. Garcia, S.F.D.M.; Filho, A.D.; de Lamotte, D.F.; Rudkiewicz, J.L. Análise de volumes de sal em restauração estrutural: Um exemplo na Bacia de Santos. *Rev. Bras. De Geocienc.* **2012**, *42*, 433–450. [CrossRef]
21. Pietzsch, R.; Oliveira, D.M.; Tedeschi, L.R.; Queiroz Neto, J.V.; Figueiredo, M.F.; Vazquez, J.C.; de Souza, R.S. Palaeohydrology of the Lower Cretaceous Pre-Salt Lacustrine System, from Rift to Post-Rift Phase, Santos Basin, Brazil. *Palaeogeogr. Palaeoclimatol. Palaeoecol.* **2018**, *507*, 60–80. [CrossRef]
22. Schultz, L.G. Quantitative Interpretation of Mineralogical Composition from X-ray and Chemical Data for the Pierre Shale. *Geol. Surv. Prof. Pap.* **1964**, *391-C*, C1–C30.
23. Van der Marel, H.W. Quantitative Analysis of Clay Minerals and Their Admixtures. *Contrib. Mineral. Petrol.* **1966**, *12*, 96–138. [CrossRef]
24. Chung, F.H. Quantitative Interpretation of X-Ray Diffraction Patterns of Mixtures. II. Adiabatic Principle of X-ray Diffraction Analysis of Mixtures. *J. Appl. Crystallogr.* **1974**, *7*, 526–531. [CrossRef]
25. Grabowska-Olszewska, B.; Osipov, V.; Sokolov, V. *Atlas of the Microstructure of Clay Soils*, 1st ed.; Panstwowe Wydawnictwo Navkowe: Varsovia, Poland, 1984; Volume 1, ISBN 8301004142.
26. Saller, A.; Rushton, S.; Buambua, L.; Inman, K.; McNeil, R.; Dickson, J.A.D.T. Presalt Stratigraphy and Depositional Systems in the Kwanza Basin, Offshore Angola. *AAPG Bull.* **2016**, *100*, 1135–1164. [CrossRef]
27. Wright, V.P. The Mantle, CO_2 and the Giant Aptian Chemogenic Lacustrine Carbonate Factory of the South Atlantic: Some Carbonates Are Made, Not Born. *Sedimentology* **2020**, *69*, 47–73. [CrossRef]
28. Wright, V.P.; Barnett, A.J. The Textural Evolution and Ghost Matrices of the Cretaceous Barra Velha Formation Carbonates from the Santos Basin, Offshore Brazil. *Facies* **2020**, *66*, 7. [CrossRef]

29. Cuadros, J. Clay Minerals Interaction with Microorganisms: A Review. *Clay Miner.* **2017**, *52*, 235–261. [CrossRef]
30. Douglas, S.; Beveridge, T.J. Mineral Formation by Bacteria in Natural Microbial Communities. *FEMS Microbiol. Ecol.* **1998**, *26*, 79–88. [CrossRef]
31. Tosca, N.J.; Wright, V.P. Diagenetic Pathways Linked to Labile Mg-Clays in Lacustrine Carbonate Reservoirs: A Model for the Origin of Secondary Porosity in the Cretaceous Pre-Salt Barra Velha Formation, Offshore Brazil. *Geol. Soc. Lond. Spec. Publ.* **2018**, *435*, 33–46. [CrossRef]
32. Farias, F.; Szatmari, P.; Bahniuk, A.; França, A.B. Evaporitic Carbonates in the Pre-Salt of Santos Basin—Genesis and Tectonic Implications. *Mar. Pet. Geol.* **2019**, *105*, 251–272. [CrossRef]
33. Muniz, M.C.; Bosence, D.W.J. Pre-Salt Microbialites from the Campos Basin (Offshore Brazil): Image Log Facies, Facies Model and Cyclicity in Lacustrine Carbonates. *Geol. Soc. Spec. Publ.* **2015**, *418*, 221–242. [CrossRef]
34. Kirkham, A.; Tucker, M.E. Thrombolites, Spherulites and Fibrous Crusts (Holkerian, Purbeckian, Aptian): Context, Fabrics and Origins. *Sediment. Geol.* **2018**, *374*, 69–84. [CrossRef]
35. Burne, R.V.; Moore, L.S. Microbialites: Organosedimentary Deposits of Benthic Microbial Communities. *Palaios* **1987**, *2*, 241–254. [CrossRef]
36. Chafetz, H.; Barth, J.; Cook, M.; Guo, X.; Zhou, J. Origins of Carbonate Spherulites: Implications for Brazilian Aptian Pre-Salt Reservoir. *Sediment. Geol.* **2018**, *365*, 21–33. [CrossRef]
37. Claes, H.; Miranda, T.; Falcão, T.C.; Soete, J.; Mohammadi, Z.; Zieger, L.; Erthal, M.M.; Aguillar, J.; Schmatz, J.; Busch, A.; et al. Model for Calcite Spherulite Formation in Organic, Clay-Rich, Lacustrine Carbonate Shales (Barbalha Formation, Aptian, Araripe Basin, NE Brazil). *Mar. Pet. Geol.* **2021**, *128*, 104988. [CrossRef]
38. Mercedes-Martín, R.; Rogerson, M.R.; Brasier, A.T.; Vonhof, H.B.; Prior, T.J.; Fellows, S.M.; Reijmer, J.J.G.; Billing, I.; Pedley, H.M. Growing Spherulitic Calcite Grains in Saline, Hyperalkaline Lakes: Experimental Evaluation of the Effects of Mg-Clays and Organic Acids. *Sediment. Geol.* **2016**, *335*, 93–102. [CrossRef]
39. Mercedes-Martín, R.; Rao, A.; Rogerson, M.; Sánchez-Román, M. Effects of Salinity, Organic Acids and Alkalinity on the Growth of Calcite Spherulites: Implications for Evaporitic Lacustrine Sedimentation. *Depos. Rec.* **2021**, 1–22. [CrossRef]
40. Léveillé, R.J.; Fyfe, W.S.; Longstaffe, F.J. Geomicrobiology of Carbonate-Silicate Microbialites from Hawaiian Basaltic Sea Caves. *Chem. Geol.* **2000**, *169*, 339–355. [CrossRef]
41. Del Buey, P.; Cabestrero, Ó.; Arroyo, X.; Sanz-Montero, M.E. Microbially Induced Palygorskite-Sepiolite Authigenesis in Modern Hypersaline Lakes (Central Spain). *Appl. Clay Sci.* **2018**, *160*, 9–21. [CrossRef]
42. Zeyen, N.; Benzerara, K.; Li, J.; Groleau, A.; Balan, E.; Robert, J.-L.; Estève, I.; Tavera, R.; Moreira, D.; López-García, P. Formation of Low-T Hydrated Silicates in Modern Microbialites from Mexico and Implications for Microbial Fossilization. *Front. Earth Sci.* **2015**, *3*, 1–23. [CrossRef]
43. Burne, R.V.; Moore, L.S.; Christy, A.G.; Troitzsch, U.; King, P.L.; Carnerup, A.M.; Joseph Hamilton, P. Stevensite in the Modern Thrombolites of Lake Clifton, Western Australia: A Missing Link in Microbialite Mineralization? *Geology* **2014**, *42*, 575–578. [CrossRef]
44. Riding, R. Microbial Carbonates: The Geological Record of Calcified Bacterial-Algal Mats and Biofilms. *Sedimentology* **2000**, *47*, 179–214. [CrossRef]
45. Chafetz, H.S.; Guidry, S.A. Deposition and Diagenesis of Mammoth Hot Springs Travertine, Yellowstone National Park, Wyoming, U.S.A. *Can. J. Earth Sci.* **2003**, *40*, 1515–1529. [CrossRef]
46. Grasby, S.E.; van Everdingen, R.O.; Bednarski, J.; Lepitzki, D.A.W. Travertine Mounds of the Cave and Basin National Historic Site, Banff National Park. *Can. J. Earth Sci.* **2003**, *40*, 1501–1513. [CrossRef]
47. Pentecost, A.; Coletta, P. The Role of Photosynthesis and CO_2 Evasion in Travertine Formation: A Quantitative Investigation at an Important Travertine-Depositing Hot Spring, Le Zitelle, Lazio, Italy. *J. Geol. Soc. Lond.* **2007**, *164*, 843–853. [CrossRef]
48. Tutolo, B.M.; Tosca, N.J. Experimental Examination of the Mg-Silicate-Carbonate System at Ambient Temperature: Implications for Alkaline Chemical Sedimentation and Lacustrine Carbonate Formation. *Geochim. Cosmochim. Acta* **2018**, *225*, 80–101. [CrossRef]
49. Chase, J.E.; Arizaleta, M.L.; Tutolo, B.M. A Series of Data-Driven Hypotheses for Inferring Biogeochemical Conditions in Alkaline Lakes and Their Deposits Based on the Behavior of Mg and SiO_2. *Minerals* **2021**, *11*, 106. [CrossRef]
50. Millot, G. *Geology of Clays: Weathering, Sedmentology and Geochemistry*, 1st ed.; Springer: Berlin, Germany, 1970; ISBN 978-3-662-41609-9.
51. Jones, B.F. *Clay Mineral Diagenesis in Lacustrine Sediments*; Mumptom, F.A., Ed.; U.S. Geological Survey: Reston, VA, USA, 1986; Volume 1578.
52. Galán, E.; Pozo, M. Palygorskite and Sepiolite Deposits in Continental Environments. Description, Genetic Patterns and Sedimentary Settings. In *Developments in Clay Science*; Galán, E., Singer, A., Eds.; Elsevier B.V.: Amsterdam, The Netherlands, 2011; Volume 3, pp. 125–173.
53. Tosca, N. Geochemical Pathways to Mg-Silicate Formation. In *Magnesian Clays: Characterization, Origin and Applications*; Pozo, M., Galán, E., Eds.; AIPEA Educational Series; Digilabs: Bari, Italy, 2015; ISBN 978-88-7522-093-8.
54. Lasaga, A.C. *Kinetic Theory in the Earth Sciences*; Princeton University Press: Princeton, NJ, USA, 1998; ISBN 9781400864874. [CrossRef]
55. Stumm, W. *Chemistry of the Solid Water Interface: Processes at the Mineral-Water and Particle-Water Interface in Natural Systems*, 1st ed.; John Wiley & Sons Inc.: New York, NY, USA, 1992.

56. Zhang, J.; Huang, F.; Lin, Z. Progress of Nanocrystalline Growth Kinetics Based on Oriented Attachment. *Nanoscale* **2010**, *2*, 18–34. [CrossRef]

57. Khoury, H.N.; Eberl, D.D.; Jones, B.F. Origin of Magnesium Clays from the Amargosa Desert, Nevada. *Clays Clay Miner.* **1982**, *30*, 327–336. [CrossRef]

58. Hay, R.L. Magnesium-Rich Clays of the Meerschaum Mines in the Amboseli Basin, Tanzania and Kenya. *Clays Clay Miner.* **1995**, *43*, 455–466. [CrossRef]

59. Pozo, M.; Casas, J. Origin of Kerolite and Associated Mg Clays in Palustrine-Lacustrine Environments. The Esquivias Deposit (Neogene Madrid Basin, Spain). *Clay Miner.* **1999**, *34*, 395–418. [CrossRef]

60. Deocampo, D.M.; Cuadros, J.; Wing-dudek, T.; Olives, J.; Amouric, M. Saline Lake Diagenesis as Revealed by Coupled Mineralogy and Geochemistry of Multiple Ultrafine Clay Phases: Pliocene Olduvai Gorge, Tanzania. *Am. J. Sci.* **2009**, *309*, 834–868. [CrossRef]

61. Jones, B.F.; Galán, E. Sepiolite and Palygorskite. *Rev. Mineral. Geochem.* **1988**, *19*, 631–674.

62. Stoessell, R.K. 25 °C and 1 Atm Dissolution Experiments of Sepiolite and Kerolite. *Geochim. et Cosmochim. Acta* **1988**, *52*, 365–374. [CrossRef]

63. Tosca, N.J.; Masterson, A.L. Chemical Controls on Incipient Mg-Silicate Crystallization at 25 °C: Implications for Early and Late Diagenesis. *Clay Miner.* **2014**, *49*, 165–194. [CrossRef]

64. Pietzsch, R.; Tedeschi, L.R.; Oliveira, D.M.; dos Anjos, C.W.D.; Vazquez, J.C.; Figueiredo, M.F. Environmental Conditions of Deposition of the Lower Cretaceous Lacustrine Carbonates of the Barra Velha Formation, Santos Basin (Brazil), Based on Stable Carbon and Oxygen Isotopes: A Continental Record of PCO$_2$ during the Onset of the Oceanic Anoxic Event 1a (OAE 1a) Interval? *Chem. Geol.* **2020**, *535*, 119457. [CrossRef]

65. Szatmari, P.; Milani, E.J. Tectonic Control of the Oil-Rich Large Igneous-Carbonate-Salt Province of the South Atlantic Rift. *Mar. Pet. Geol.* **2016**, *77*, 567–596. [CrossRef]

66. Badaut, D.; Risacher, F. Authigenic Smectite on Diatom Frustules in Bolivian Saline Lakes. *Geochim. Cosmochim. Acta* **1983**, *41*, 363–375. [CrossRef]

67. Darragi, F.; Tardy, Y. Authigenic Trioctahedral Smectites Controlling PH, Alkalinity, Silica and Magnesium Concentrations in Alkaline Lakes. *Chem. Geol.* **1987**, *63*, 59–72. [CrossRef]

68. Martín de Vidales, J.L.; Pozo, M.; Casas, J. Evidences of Stevensite Formation from Kerolite/Stevensite Mixed Layers. Influence of Alkalinity and Silica Activities. In *Advances in Clay Minerals*; Ortega-Huertas, M., López-Galindo, A., Palomo-Delgado, I., Eds.; Sociedade Española de Arcillas: Granada, Spain, 1996; pp. 134–136; ISBN 84-8499-482-1.